Editors' Suggestion

Inferring tree structure with hidden traps from first-passage times

Fabian H. Kreten, Ludger Santen, and Reza Shaebani*
Department of Theoretical Physics and Center for Biophysics, Saarland University, 66123 Saarbrücken, Germany

(Received 21 May 2025; accepted 9 October 2025; published 10 November 2025)

Tracking the movement of tracer particles has long been a strategy for uncovering complex structures. Here, we study discrete-time random walks on finite Cayley trees to infer key parameters such as tree depth and geometric bias toward the root or leaves. By analyzing first-passage properties, we show that the first two first-passage-time factorial moments (FPTFMs) uniquely determine the tree structure. However, if the random walker experiences waiting phases—due to sticky branch walls or presence of traps—then this identification becomes nontrivial. We demonstrate that the generating function of the first-passage-time (FPT) distribution decomposes into contributions from the waiting-time distribution and the random walk without waiting, leading to a nonlinear system of equations relating the factorial moments of the waiting-time distribution and the FPTFMs of random walks with and without waiting. For geometrically distributed waiting times, additional moment measurements do not suffice, but unique determination of the structure is achieved by varying initial conditions or fitting the Fourier transform of the FPT distribution to measured data. The latter method remains effective also for power-law waiting-time distributions, where higher-order FPTFMs are undefined. These results provide a framework for reconstructing treelike networks from FPT data, with applications in biological transport and spatial networks.

DOI: 10.1103/hh42-b48p

I. INTRODUCTION

Tracking the movement of tracer particles has long been a practical method for probing the unknown structure and topology of labyrinthine environments, ranging from disordered media to biological transport networks [1–14]. For instance, diffusion propagators have been used to estimate structural characteristics of porous media, including porosity, confinement, permeability, absorption strength, and surface-to-volume ratio [2–5]. Other examples include identifying magnetic bubble arrangements through the anomalous behavior of the mean-square displacement of paramagnetic colloids in flashing magnetic potentials [6], or determining the geometry of absorbing boundaries—such as those in acoustic cavities—from the eigenvalue spectrum of the confined diffusion equation [7].

Analyzing diffusive dynamics, e.g., by measuring the diffusion constant or mean-square displacement, typically requires direct tracking of the tracer, which can pose technical challenges or necessitate invasive methods in biological or medical contexts. Moreover, such measures often fail to capture fine structural details. As an alternative, other transport quantities have been employed to indirectly assess the structural characteristics of interest. For instance, the absorption efficiency of diffusing oxygen can reflect the topology of the bronchial tree in the human lung [8], or the mean free path of light relates to obstacle size and density in turbid media [9], enabling the use of diffusive light propagation to probe the temporal structural evolution of foams and opaque environments [10,11]. Among other measurable quantities, first-passage-time (FPT) properties offer promising tools for indirect structural analysis. For example, the first return time of random walks has been used to estimate geometrical properties of complex networks, including the number of triangles, loops, and subgraphs [12]. Similarly, the mean time for reactants to reach a reaction center or to encounter each other can predict the timescale of autocatalytic reactions on inhomogeneous substrates [13].

Our study focuses on treelike structures, which represent a broad range of real-world systems—from synthetic polymer configurations and dendrimer macromolecules to the bronchial architecture of lungs, vascular networks, neuronal dendrites, as well as certain communication and power distribution networks, and river basins [8,14–26]. Treelike architectures are also highly relevant in network and graph theory, epidemic modeling, and computational search algorithms [27–31]. Regular finite Cayley trees and infinite Bethe lattices have been thoroughly studied by mapping them onto effective one-dimensional (1D) lattices [32–40], enabling the calculation of stochastic quantities of interest, such as the probability of return to the origin and the mean first-passage-time (MFPT) to reach a target node. The latter has been shown to depend on both the size of the tree and the bias in hopping toward the target. Consequently, measuring the MFPT alone is typically insufficient to uniquely determine the structure of even simple Cayley trees. While it has been proposed that using random walkers with varying waiting-time statistics may aid in structural inference [34], such waiting is

*Contact author: shaebani@lusi.uni-sb.de

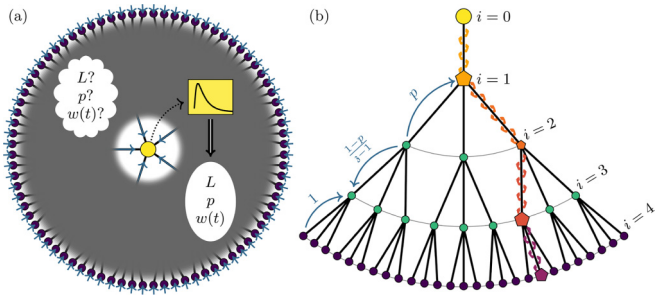

FIG. 1. Schematic illustration of the problem and modeling framework. (a) A Cayley tree of unknown structure (represented by the gray shading), characterized by its depth L, upward hopping probability p (in conjunction with the coordination number $\mathfrak{z}$), and the distribution $w(t)$ of waiting times induced by stickiness or hidden traps along the branch walls. Random walkers are released from a specific level of the tree—here, the leaf nodes (dark purple)—and eventually reach the root (yellow). The distribution of their first-passage times (inset graph) is used to infer the structural parameters L, p, and $w(t)$. (b) A single subtree of a Cayley tree of depth $L = 4$ and coordination number $\mathfrak{z} = 4$. The leaf nodes ($i = L = 4$) are displayed in dark purple, the root node ($i = 0$) in yellow. Transition probabilities are indicated on the left. On the right, a sample trajectory of a walker moving from a leaf to the root is depicted with footsteps and pentagons; the size of each pentagon reflects the random waiting time at that node, while the color of the pentagons and footsteps transitions from purple to yellow to indicate the progression of time. A cycle-free sample path is chosen to clearly illustrate the waiting behavior.

often an inherent property of the system—originating from stickiness or hidden traps along the tree branches—rather than a characteristic of the random walker itself. Here, we are particularly interested in predicting the structure of more intricate, nonuniform (depth-dependent) trees—such as those that thin or thicken toward the root—and under the influence of inherent stochastic waiting events along the branches. We adopt discrete-time random walks on finite Cayley trees as an analytically tractable framework for studying such branched structures. While continuous-time random walks are a widely used alternative, we focus on a discrete-time approach, which naturally captures stepwise processes, such as sequential movement in biological systems or signal propagation in networks.

We employ a FPT-based analysis as a powerful tool for inferring structural parameters of the system—such as the bias in movement toward the root or the frequency of temporary sticking and trapping along the path—as illustrated in Fig. 1(a). We demonstrate that knowing two first-passage-time factorial moments (FPTFMs) for tracer particles to reach the root of a Cayley tree is sufficient to uniquely determine the structure of the tree in the absence of traps. We then extend our approach to incorporate waiting times resulting from the presence of traps. In this case, the generating function of the FPT distribution of the random walk can be written as the composition of the generating function of the FPT distribution of a walk without delay and the generating function of the waiting-time distribution. This decomposition can yield a nonlinear system of equations that relates factorial moments of the waiting-time distribution and the FPTFMs of walks with and without trapping effects. We show that accurate inference of the tree structure in such cases requires more refined analysis—such as probing with varied initial conditions or fitting the Fourier transform of the FPT distribution to observed data. Notably, our method remains effective even in the presence of power-law distributed waiting times, where higher-order FPTFMs may diverge.

The remainder of the paper is organized as follows. In Sec. II, we introduce the mathematical formulation of the problem and derive the generating function relations for FPTs without and with waiting times, respectively. Sections III and IV consider the FPTFM-based inference of structural parameters in absence and presence of waiting. Section V presents the inference framework using the Fourier transform of the FPT distribution and examines the impact of different waiting-time distributions. Finally, Sec. VI summarizes the main findings and concludes the paper.

II. METHOD

In this section, we establish the mathematical framework underlying our analysis. A central tool throughout is the use of generating functions, widely employed in the study of combinatorial sequences [41–43] and the probability distributions of discrete random variables [44]. Given a sequence $(a(n))_{n\geqslant 0}$, its ordinary generating function is defined by the power series $\hat{a}(z) = \sum_{n=0}^{\infty} a(n)\, z^n$. Throughout this work, we use a hat to denote the generating function of the corresponding quantity. We use the symbol $\overset{\text{ogf}}{\longleftrightarrow}$ to indicate the correspondence between relations in the sequence domain and their ordinary generating function counterparts. A particularly useful property of ordinary generating functions is the convolution property [42], which states that for k sequences $(a_1(n))_{n\geqslant 0},\ \ldots,\ (a_k(n))_{n\geqslant 0}$, the convolution satisfies

$$b(n) = \sum_{n_1+\ldots+n_k=n} a_1(n_1)\cdots a_k(n_k) \overset{\text{ogf}}{\longleftrightarrow} \hat{b}(z) = \prod_{i=1}^{k} \hat{a}_i(z), \quad (1)$$

where the sum runs over all k-tuples $(n_1,\ \ldots,\ n_k) \in \mathbf{N}^k$ such that $n_1 + \cdots + n_k = n$.

The second key tool used in this paper is the factorial moment, a well-established quantity for studying nonnegative integer-valued random variables and their distributions [41,44]. Factorial moments have also seen applications in data analysis, particularly in high-energy physics [45]. Let $t^{\underline{k}} = \prod_{n=0}^{k-1}(t-n)$ denote the kth falling factorial, with the convention $t^{\underline{0}} = 1$. Then, for a random variable t with the probability distribution $f(t)$ the expectation value of the kth falling factorial defines the kth factorial moment $\langle t^{\underline{k}}\rangle$ of t. A property which makes factorial moments more convenient that ordinary moments is that they are directly generated by derivatives of the generating function $\hat{f}(z)$ of the probability distribution:

$$\langle t^{\underline{k}}\rangle = \left.\frac{\mathrm{d}^k \hat{f}}{\mathrm{d}z^k}\right|_{z=1}. \quad (2)$$

Since monomials can be expressed in terms of falling factorials, factorial and ordinary moments, $\langle t^{\underline{n}}\rangle$ and $\langle t^n\rangle$, are

related to each other via $\langle t^{\underline{n}}\rangle = \sum_{k=0}^{n}(-1)^{n-k}\left[{n \atop k}\right]\langle t^k\rangle$ and $\langle t^n\rangle = \sum_{k=0}^{n}\left\{{n \atop k}\right\}\langle t^{\underline{k}}\rangle$, where $\left[{n \atop k}\right]$ and $\left\{{m \atop k}\right\}$ denote the (unsigned) Stirling numbers of first and second kind [43].

A. Recurrence relation for FPTFMs

Having introduced factorial moments, we now derive a recurrence relation for the FPTFMs. Notably, this derivation does not rely on any assumptions about the random walk taking place on a tree structure; it holds for arbitrary discrete random walks on possibly infinite state spaces. Furthermore, extending the approach to continuous spaces is straightforward and likely requires only minimal adaptation.

A well-established approach for obtaining the first-passage-time distribution $f(t)$ is through the survival probability $S(t)$, which denotes the probability that the walker has not reached the target by time t. The relation between these two quantities, as well as between their generating functions, is given by $f(t+1) = S(t) - S(t+1) \overset{\text{ogf}}{\longleftrightarrow} \hat{f}(z) = (z-1)\hat{S}(z) + 1$ [35]. Applying Eq. (2) to this relation allows one to express the FPTFMs in terms of the survival probability:

$$\frac{1}{k}\langle t^{\underline{k}}\rangle = \frac{\mathrm{d}^{k-1}}{\mathrm{d}z^{k-1}}\hat{S}\bigg|_{z=1}. \tag{3}$$

This framework can be directly applied to Markovian random walks in discrete time, as considered in the following. Let $\mathbf{P}(t)$ denote the vector (or sequence) of occupation probabilities for all states at time t. The time evolution of $\mathbf{P}$ is governed by the Chapman-Kolmogorov equation $\mathbf{P}(t+1) = \mathsf{M}\,\mathbf{P}(t)$, where M is the transition matrix. If M respects the absorbing nature of the target sites, then the survival probability vector $\mathbf{S}(t)$, whose entries correspond to the survival probability from each starting site, evolves according to the backward equation $\mathbf{S}(t+1) = \mathsf{M}^\dagger\mathbf{S}(t) \overset{\text{ogf}}{\longleftrightarrow} -1 = (z\mathsf{M}^\dagger - 1)\hat{\mathbf{S}}(z)$, where $\mathsf{M}^\dagger$ is the transpose of M. Applying Eq. (3) to this relation yields the following recurrence for the FPTFMs:

$$-k\mathsf{M}^\dagger\langle \mathbf{t}^{\underline{k-1}}\rangle = (\mathsf{M}^\dagger - 1)\langle \mathbf{t}^{\underline{k}}\rangle \quad \text{for } k > 0, \tag{4}$$

where $\langle \mathbf{t}^{\underline{k-1}}\rangle$ is the vector of FPTFMs indexed over the starting sites. This relation serves as the discrete-time analog of a well-known identity for ordinary moments in continuous-time processes [46].

B. Decoupling the FPT distribution for walks with waiting

Next, we derive the relation between the ordinary generating function of the FPT distribution for a discrete-time random walk with site-independent waiting and that of a walk without waiting, along with the generating function of the waiting-time distribution. This decoupling approach parallels well-known results obtained in continuous time and space using Laplace transforms [47], and in discrete space using cumulant generating functions [48], but is here expressed directly in terms of ordinary generating functions.

Let $f(t)$ denote the FPT distribution for a random walk with independent and identically distributed (i.i.d.) waiting times drawn from the distribution $w(t)$ at each site. Let $\mathfrak{f}(t)$ be the FPT distribution of the same walk without waiting times (i.e., $w(t) = \delta_{t,1}$). Then, $f(t)$ is given by

$$f(t) = \sum_{k=0}^{\infty}\mathfrak{f}(k)\sum_{\tau_1+\cdots+\tau_k=t} w(\tau_1)\cdots w(\tau_k), \tag{5}$$

and applying the convolution property of ordinary generating functions, Eq. (1), the generating function of $f(t)$ becomes

$$\hat{f}(z) = \sum_{k=0}^{\infty}\mathfrak{f}(k)\hat{w}(z)^k = \hat{\mathfrak{f}}(\hat{w}(z)), \tag{6}$$

i.e., the composition of the ordinary generating functions of the FPT distribution without waiting and the waiting-time distribution.

Applying Eq. (3) to Eq. (6) and using the normalization condition $\hat{w}(1) = 1$ for probability distributions, one can express the FPTFMs with waiting $\langle t^{\underline{k}}\rangle$ in terms of the FPTFMs without waiting $\langle \mathfrak{t}^{\underline{k}}\rangle$ and the factorial moments of the waiting-time distribution $\langle \tau_w^{\underline{k}}\rangle$:

$$\begin{aligned}
\langle t^{\underline{1}}\rangle &= \langle \mathfrak{t}^{\underline{1}}\rangle\langle \tau_w^{\underline{1}}\rangle,\\
\langle t^{\underline{2}}\rangle &= \langle \mathfrak{t}^{\underline{2}}\rangle\langle \tau_w^{\underline{1}}\rangle^2 + \langle \mathfrak{t}^{\underline{1}}\rangle\langle \tau_w^{\underline{2}}\rangle,\\
\langle t^{\underline{3}}\rangle &= \langle \mathfrak{t}^{\underline{3}}\rangle\langle \tau_w^{\underline{1}}\rangle^3 + 3\langle \mathfrak{t}^{\underline{2}}\rangle\langle \tau_w^{\underline{1}}\rangle\langle \tau_w^{\underline{2}}\rangle + \langle \mathfrak{t}^{\underline{1}}\rangle\langle \tau_w^{\underline{3}}\rangle,\\
&\vdots\\
\langle t^{\underline{m}}\rangle &= \sum_{\mathbf{b}\in B_m} M_{\mathbf{b}}^m\langle \mathfrak{t}^{\underline{\|\mathbf{b}\|_1}}\rangle\prod_{k=1}^{m}\left(\frac{\langle \tau_w^{\underline{k}}\rangle}{k!}\right)^{b_k}.
\end{aligned} \tag{7}$$

The last line represents the general form obtained using Faà di Bruno's formula; see the Appendix for details. Here $B_m = \{\mathbf{b}\in\mathbf{N}^m;\ \sum_{k=1}^{m} kb_k = m\}$, $M_{\mathbf{b}}^m = \frac{m!}{\prod_{k=1}^{m} b_k!}$ a generalized multinomial coefficient [49], and $\|\mathbf{b}\|_1 = \sum_{k=1}^{m} b_k$. We note that $\|\mathbf{b}\|_1 \leqslant m$, with equality $\|\mathbf{b}\|_1 = m$ if and only if $\mathbf{b} = (m, 0, \ldots, 0)$. Due to its complexity, the general expression is primarily useful for theoretical purposes, while the finite number of moments typically required in applications can be computed manually or with the aid of a computer algebra system. In the following, we use the unified notation $\langle \tau_w^{\underline{k}}\rangle$ for the factorial moments of the waiting-time distribution, $\langle t^{\underline{k}}\rangle$ for the FPTFMs with waiting, and $\langle \mathfrak{t}^{\underline{k}}\rangle$ for the FPTFMs without waiting. Moreover, the index i is used for the FPTFMs with/without waiting, $\langle t_i^{\underline{k}}\rangle$ and $\langle \mathfrak{t}_i^{\underline{k}}\rangle$, if starting from level i.

C. Cayley trees and random walks thereon

To conclude this section, we introduce Cayley trees and apply the general results of the preceding subsections to random walks on such structures. We then outline the waiting-time distributions considered in this work and comment on the connection between the generating function and the Fourier transform of the FPT distribution.

The random walk takes place on a finite Cayley tree of depth L, which is a regular cycle-free graph constructed as follows: The root node is assigned to level or shell $i = 0$. It connects to $\mathfrak{z}$ child nodes, forming level $i = 1$. For levels $0 < i < L$, each node at level i is connected to $\mathfrak{z} - 1$ nodes forming the level $i+1$. The parameter $\mathfrak{z}$ denotes the coordination number of the tree [50]; see Fig. 1(b).

The random walk proceeds as follows: At each node on levels $0 < i < L$, the walker moves to the parent node at level $i-1$ with probability p, and to each of the $\mathfrak{z}-1$ child nodes at level $i+1$ with probability $\frac{1-p}{\mathfrak{z}-1}$. At the leaves ($i=L$), the walker always moves to the parent level ($i=L-1$) with probability 1. The dynamics at the root ($i=0$) are irrelevant for computing FPTs to it, and we treat it as an absorbing state to facilitate the use of the adjoint (backward) equation formalism. For unbiased diffusion on a Cayley tree, the rootward transition probability p is simply related to the branching parameter $\mathfrak{z}$ by $p=\frac{1}{\mathfrak{z}}$. In the presence of a bias or an energy difference ΔE between consecutive levels, this relation is modified to $p=\frac{1}{1+(\mathfrak{z}-1)\exp(-\Delta E/k_B T)}$, with k_B denoting Boltzmann constant [23]. Possible sources of such bias include shortest-path preferences or morphological tapering, as observed in dendritic trees of neurons [14]. For this reason, we treat p as a tunable parameter, which allows the formalism to remain general and applicable to both unbiased and biased scenarios.

Since our primary interest lies in the first-passage time to the root, and the transition probabilities are identical for all nodes at a given level, the dynamics can be effectively reduced to a one-dimensional process over levels rather than individual nodes [32–40]. This reduction renders the transition matrix

$$\mathsf{M}=\begin{pmatrix} 1 & p & & & & & \\ 0 & 0 & p & & & & \\ & 1-p & 0 & \ddots & & & \\ & & \ddots & \ddots & p & & \\ & & & 1-p & 0 & 1 & \\ & & & & 1-p & 0 & \end{pmatrix} \tag{8}$$

tridiagonal, significantly simplifying the computation of the FPTFMs $\langle \mathsf{t}_i^{\underline{k}} \rangle$ from any level i to the root in $\mathcal{O}(L\,k)$ time using Eq. (4). For target sites other than the root, reduction to one dimension is not possible anymore and the transition matrix for the full tree must be considered.

Furthermore, the generating function of the FPT probability distribution $\hat{\mathfrak{f}}_L(z;L)=\sum_{t=0}^{\infty}\mathfrak{f}_L(t;L)z^t$ to the root for a random walker starting at level L (the leaves, denoted by the index) of a tree of depth L (denoted by the second argument) has been derived previously [14,34]. Adapting their result to our setting without waiting times, and using the abbreviation $A(z)=\sqrt{1-4(1-p)pz^2}$, the expression reads

$$\hat{\mathfrak{f}}_L(z;L)=\frac{2^{L+1}p^L z^L A(z)}{(1+A(z))^L(2p-(1-A(z)))-(1-A(z))^L(2p-(1+A(z)))}. \tag{9}$$

Since $A(z)$ is an even function and the denominator of $\hat{\mathfrak{f}}_L(z;L)$ is odd in A, $\hat{\mathfrak{f}}(z;L)$ has the same parity as L. Consequently, the FPT probability distribution $\mathfrak{f}_L(t;L)$ vanishes for all t that are not of the same parity as L. This behavior is expected because the tree with the transition rules defined in Eq. (8) forms a bipartite network and the walker alternates between the two parts in every step. Hence, it requires an even number of steps to reach the root once it has entered the part containing the root.

Note that for $L>1$, the decomposition of the time to reach the root starting from the leaves into the time to reach the level below the root starting from the leaves and the time to reach the root starting from the level below, i.e., $T_{L\to 0}=T_{L\to 1}+T_{1\to 0}$, holds and that $T_{L\to 1}$ and $T_{1\to 0}$ are distributed according to $\mathfrak{f}_{L-1}(t;L-1)$ and $\mathfrak{f}_1(t;L)$. Using Eqs. (1) and (9), the generating function of the FPT distribution to reach the root starting from the level below can be obtained as

$$\hat{\mathfrak{f}}_1(z;L)=\frac{\hat{\mathfrak{f}}_L(z;L)}{\hat{\mathfrak{f}}_{L-1}(z;L-1)}. \tag{10}$$

Using Eqs. (2), (9), and (10), one can in principle derive explicit expressions for the corresponding factorial moments. However, due to the complexity of the resulting formulas, we do not pursue this route further here.

We consider two waiting-time distributions in this paper, both supported on the set of positive integers $t\geqslant 1$. The first one is the geometric distribution

$$w(t)=q(1-q)^{t-1}\overset{\text{ogf}}{\longleftrightarrow}\hat{w}(z)=\frac{qz}{1-(1-q)z}, \tag{11}$$

which arises in the context of random walks with spontaneous stepping with probability q. The second one is the zeta distribution, defined by

$$w(t)=\frac{t^{-s}}{\mathrm{Li}_s(1)}\overset{\text{ogf}}{\longleftrightarrow}\hat{w}(z)=\frac{\mathrm{Li}_s(z)}{\mathrm{Li}_s(1)}, \tag{12}$$

where $s>1$ and $\mathrm{Li}_s(z)=\sum_{t\geqslant 1}t^{-s}z^t$ denotes the Polylogarithm function. This distribution is considered in Sec. V. For the zeta distribution, only the (factorial) moments up to order $s-1$ are finite. In the numerical calculations presented in Sec. V, the polylogarithm function must be evaluated for real parameters s and complex arguments z; suitable numerical libraries are available for this purpose [51].

For the analysis in Sec. V, the discrete-time Fourier transform (DTFT) of the FPT distribution $\tilde{f}(\omega)$ is required. This quantity is readily obtained from the generating function $\hat{f}(z)$ of the FPT distribution via $\tilde{f}(\omega)=\sum_{t\geqslant 0}f(t)\mathrm{e}^{-\mathrm{i}\omega t}=\hat{f}(\mathrm{e}^{-\mathrm{i}\omega})$. Moreover, sampling the DTFT at regularly spaced points $k=0,\ldots,N-1$ around the unit circle and applying the inverse discrete-time Fourier transform provides a method to numerically invert the generating function and recover the FPT distribution [52,53]. Figure 2 shows representative FPT distributions and their corresponding DTFTs for various parameter sets.

Each contour in Figs. 2(e)–2(h) encloses the origin and loops exactly L times, reflecting the depth of the tree. This can be understood by a continuity argument. For a tree of depth L with walkers starting from the leaves, the earliest possible arrival time is $t=L$ and the generating function of the FPT distribution $\hat{\mathfrak{f}}_L(z;L)$ has its lowest nonzero contribution at order z^L. Hence, for small radii $\rho\ll 1$ the image of the

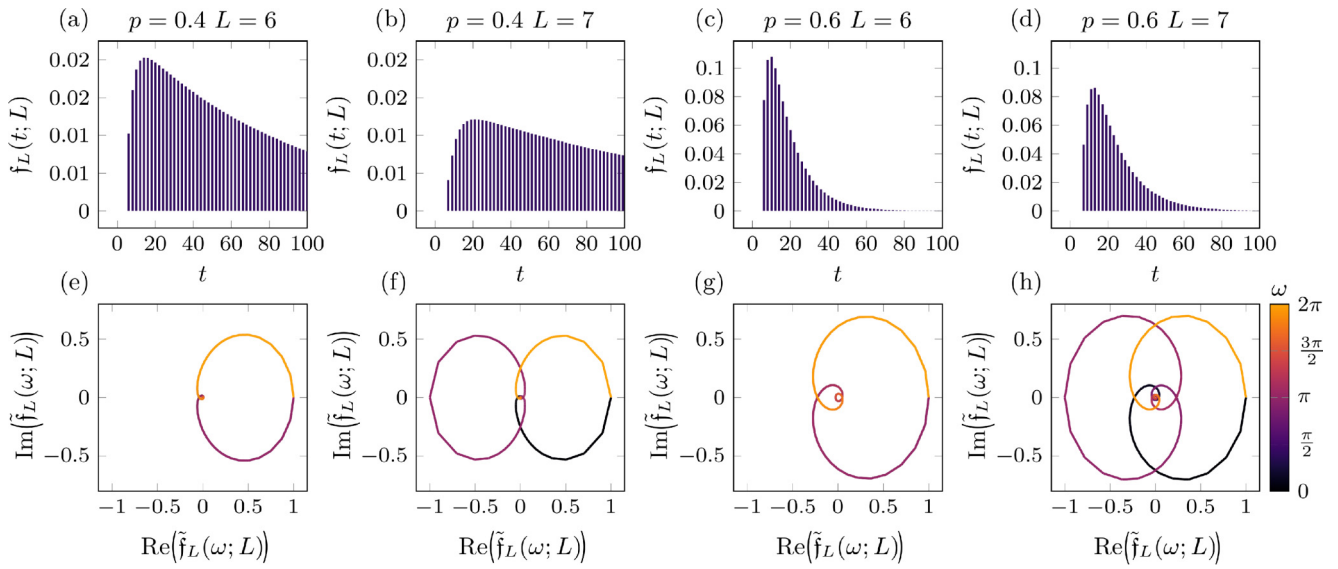

FIG. 2. First-passage-time distributions and their Fourier transforms for random walks on regular trees without waiting. (a)–(d) Examples of the FPT distribution $\mathfrak{f}_L(t;L)$ from the leaves to the root of a regular Cayley tree, for a random walker without waiting times. $\mathfrak{f}_L(t;L)$ is nonzero for $t \geqslant L$ and only for even or odd t depending on L. (e)–(h) Fourier transforms $\tilde{\mathfrak{f}}_L(\omega;L)$ of the corresponding FPT distributions [from panels (a)–(d)], shown in the complex plane. Each contour encloses the origin and loops exactly L times. For even values of L, the contour is traced twice. The parameters L and p used for each column are indicated at the top.

circle $|z| = \rho$ under $\hat{\mathfrak{f}}_L(z;L)$ is approximately parameterized by $s \mapsto e^{-iLs}$, which winds L times around the origin as s varies from 0 to 2π. By continuity, increasing ρ up to 1 leaves this winding number unchanged, which explains why the contours—corresponding to images of the unit circle under $\hat{\mathfrak{f}}_L(z;L)$—in Figs. 2(e)–2(h) loop exactly L times.

III. RANDOM WALK WITHOUT WAITING

With the theoretical groundwork established, we now turn to the task of inferring structural properties of Cayley trees from FPT statistics. We begin with the case of a random walk without waiting times. In this setting, the phase space of the Cayley tree is fully determined by two parameters: the tree depth L, and the bias probability p, which may implicitly encode the coordination number $\mathfrak{z}$. Consequently, the FPT distribution and its moments depend only on L and p. This implies that, in principle, two independent observables derived from FPT statistics should suffice to uniquely identify these parameters.

In Fig. 3(a), the phase diagram of the first factorial moment $\langle \mathfrak{t}_L^1 \rangle$ is shown, and in Fig. 3(c), the normalized second factorial moment $\frac{\langle \mathfrak{t}_L^2 \rangle}{\langle \mathfrak{t}_L^1 \rangle^2}$ is plotted for random walkers starting from the leaves. Across most of the phase space, the contour lines of constant $\langle \mathfrak{t}_L^1 \rangle$ and $\frac{\langle \mathfrak{t}_L^2 \rangle}{\langle \mathfrak{t}_L^1 \rangle^2}$ intersect at a unique point, which identifies the corresponding parameters p and L; cf. Fig. 3(e). The only exception occurs in the regime of low p and high L where $\frac{\langle \mathfrak{t}_L^2 \rangle}{\langle \mathfrak{t}_L^1 \rangle^2}$ saturates. This ambiguity can be resolved by additionally considering the first FPTFM $\langle \mathfrak{t}_1^1 \rangle$. Including another initial condition introduces additional overhead in measuring the factorial moments, as it requires conducting an extra experiment for each added initial condition. The relation $\langle \mathfrak{t}_{L,L}^1 \rangle = \langle \mathfrak{t}_{1,L}^1 \rangle + \langle \mathfrak{t}_{L-1,L-1}^1 \rangle$ [which follows from Eq. (10)] links the first FPTFM from the level below the root to those from the leaves in trees of depths $L-1$ and L as denoted by the second index. Moreover, if particles are allowed to leave the root, then $\langle \mathfrak{t}_1^1 \rangle$ corresponds to the mean return time to the root minus the mean time it takes to leave it. Together, these relations offer a way to avoid conducting a second experiment, provided it is possible to determine whether a particle has already reached the root or the level below. This could be achieved, for instance, by marking or using distinguishable particles.

Figures 3(b) and 3(d) show phase diagrams of the first FPTFM $\langle \mathfrak{t}_1^1 \rangle$ (starting from the level below the root) and the ratio $\frac{\langle \mathfrak{t}_1^1 \rangle}{\langle \mathfrak{t}_L^1 \rangle}$. When plotting the contour lines of $\langle \mathfrak{t}_1^1 \rangle$ and $\frac{\langle \mathfrak{t}_1^1 \rangle}{\langle \mathfrak{t}_L^1 \rangle}$ in a single coordinate system, as in Fig. 3(f), they intersect at unique points—even in the regime where $\frac{\langle \mathfrak{t}_L^2 \rangle}{\langle \mathfrak{t}_L^1 \rangle^2}$ saturates. Since $\langle \mathfrak{t}_1^1 \rangle$ and $\langle \mathfrak{t}_L^1 \rangle$ exhibit similar dependence on the parameters, they can be used interchangeably in the preceding inference framework. This demonstrates that, depending on the tree depth L and the bias probability p, either the first two FPTFMs from the same starting point or the first FPTFMs from two different initial conditions suffice to uniquely determine p and L. We note that Fig. 9 in the Appendix also presents the same analysis as Fig. 3, but restricted to the regime $p \geqslant 0.5$, allowing the use of contour levels with narrower spacing.

A transition in the behavior of the factorial moments occurs at the bias value $p = 0.5$ for deep trees. For example, the first factorial moment starting from the deepest level (corresponding to the mean escape time from regular trees of depth L

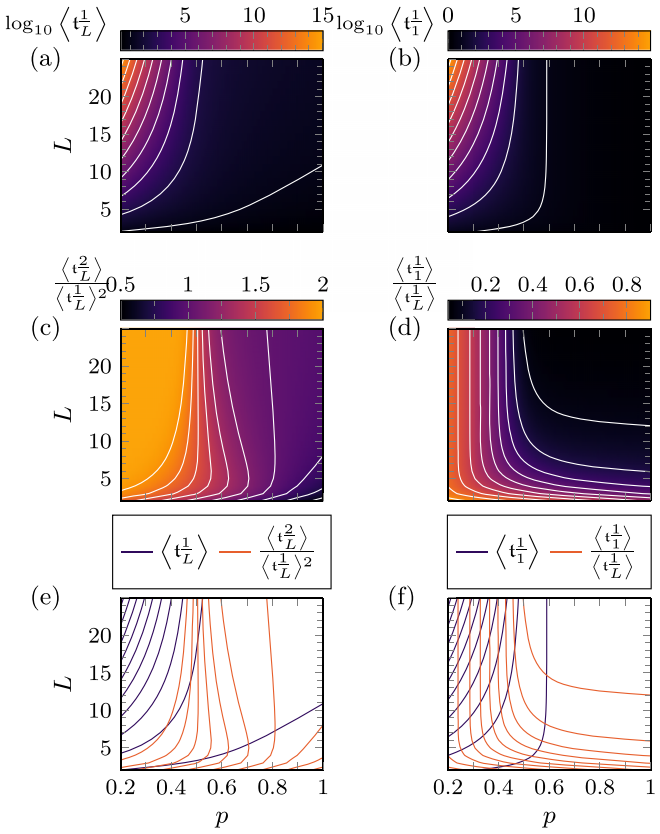

FIG. 3. First-passage-time factorial moments as functions of tree depth L and upward hopping bias p. (a), (b) Logarithm of the first factorial moment for walkers starting from the leaf nodes [$\log_{10}\langle \mathfrak{t}_L^1\rangle$, panel (a)] or starting one level below the root [$\log_{10}\langle \mathfrak{t}_1^1\rangle$, panel (b)]. Lines are contours of constant $\log_{10}\langle \mathfrak{t}_L^1\rangle$ or $\log_{10}\langle \mathfrak{t}_1^1\rangle$, respectively. (c) Normalized second factorial moment $\frac{\langle \mathfrak{t}_L^2\rangle}{\langle \mathfrak{t}_L^1\rangle^2}$ for walkers starting from the leaves. This quantity saturates at large L and small p, limiting its utility for parameter inference in that regime. (d) Ratio $\frac{\langle \mathfrak{t}_1^L\rangle}{\langle \mathfrak{t}_L^1\rangle}$, comparing first factorial moments for walkers starting just below the root versus from the leaves. This ratio becomes independent of L for small p and sufficiently deep trees, making it a robust alternative for inferring tree parameters when the normalized second moment is saturated. (e), (f) Contour plots showing combinations of moment-based observables. In panel (e), contours of $\log_{10}\langle \mathfrak{t}_L^1\rangle$ and $\frac{\langle \mathfrak{t}_L^2\rangle}{\langle \mathfrak{t}_L^1\rangle^2}$ intersect at a unique point corresponding to the true values of L and p. Similarly, panel (f) shows that intersections of $\log_{10}\langle \mathfrak{t}_1^1\rangle$ and $\frac{\langle \mathfrak{t}_1^L\rangle}{\langle \mathfrak{t}_L^1\rangle}$ contours provide an alternative route to identify the tree parameters.

studied in Ref. [40]) can be written as

$$\langle \mathfrak{t}_L^1\rangle = \frac{L}{2p-1} + \frac{1-p}{(2p-1)^2}\left[\left(\frac{1-p}{p}\right)^L - 1\right]. \tag{13}$$

For deep trees, this expression exhibits two distinct regimes depending on the bias parameter p: linear scaling with L when $p > \frac{1}{2}$, and exponential growth with L when $p < \frac{1}{2}$:

$$\langle \mathfrak{t}_L^1\rangle \overset{L\gg 1}{\simeq} \begin{cases} \frac{L}{2p-1}, & p > \frac{1}{2}, \\ \frac{1-p}{(2p-1)^2}\left(\frac{1-p}{p}\right)^L, & p < \frac{1}{2}. \end{cases} \tag{14}$$

Thus, $p = 0.5$ marks the crossover point between qualitatively different scaling behaviors. Owing to the recurrence relation (4), it is natural to expect that higher factorial moments display a similar crossover at the same bias value.

IV. RANDOM WALK WITH WAITING

We now turn to the case in which the random walker experiences waiting times. These delays could be caused by traps along the links between nodes, but even in the absence of such traps, geometric waiting can serve as a simple way to model diffusive travel time between nodes. While we treat the process as discrete hopping, we emphasize that—with an appropriate waiting-time distribution $w(t)$—all results remain valid if the walker moves continuously along the links and the process of the last visited node is considered.

A priori, the kth FPTFM of a walk with waiting $\langle t^k\rangle$, as given by Eq. (7), depends on $2k$ quantities: the first k FPTFMs of the walk without waiting $\langle \mathfrak{t}^k\rangle$, and the first k moments of the waiting-time distribution $\langle \tau_w^k\rangle$. If the waiting-time moments are known (as also assumed in Ref. [34]), they can be substituted into Eq. (7), resulting in a triangular linear system of equations. Solving this system for the first two FPTFMs without waiting, $\langle \mathfrak{t}^1\rangle$ and $\langle \mathfrak{t}^2\rangle$, is straightforward, thereby reducing the problem to the previously treated case without waiting.

If the moments of the waiting-time distribution are unknown, the number of unknowns must be reduced by further assumptions. First, since the FPT distribution of the walk without waiting depends only on the two parameters p and L, only two of its factorial moments $\langle \mathfrak{t}^k\rangle$ are independent. This limits the number of unknowns in Eq. (7) to $\min(2,k)+k$. To reduce the number of unknowns further—ideally to match the number of equations—one must assume or know a specific parametric form of the waiting-time distribution $w(t)$. If $w(t)$ depends on ℓ parameters, then only ℓ of its factorial moments $\langle \tau_w^k\rangle$ are independent. Therefore, a necessary condition for solvability is that $2+\ell \leqslant k$. These, however, are necessary but not sufficient conditions. As it is demonstrated by the example of a spontaneously moving walker in the following subsection, measuring first-passage moments beyond the second may still be insufficient to uniquely determine all parameters. This ambiguity can be resolved by additionally measuring the first moment of the FPT for a different initial condition.

Alternatively, following the approach of Ref. [34], instead of measuring higher-order FPTFMs, one can match the number of unknowns by measuring lower-order factorial moments under several distinct waiting scenarios. Let n be the number of different parameter sets considered for the waiting-time distribution. Then the inequality $\min(2,k)+n\min(\ell,k) \leqslant nk$ must be satisfied. It is easy to see that this inequality can only hold when $k > \ell$, i.e., more moments must be measured than there are independent moments of the waiting-time distribu-

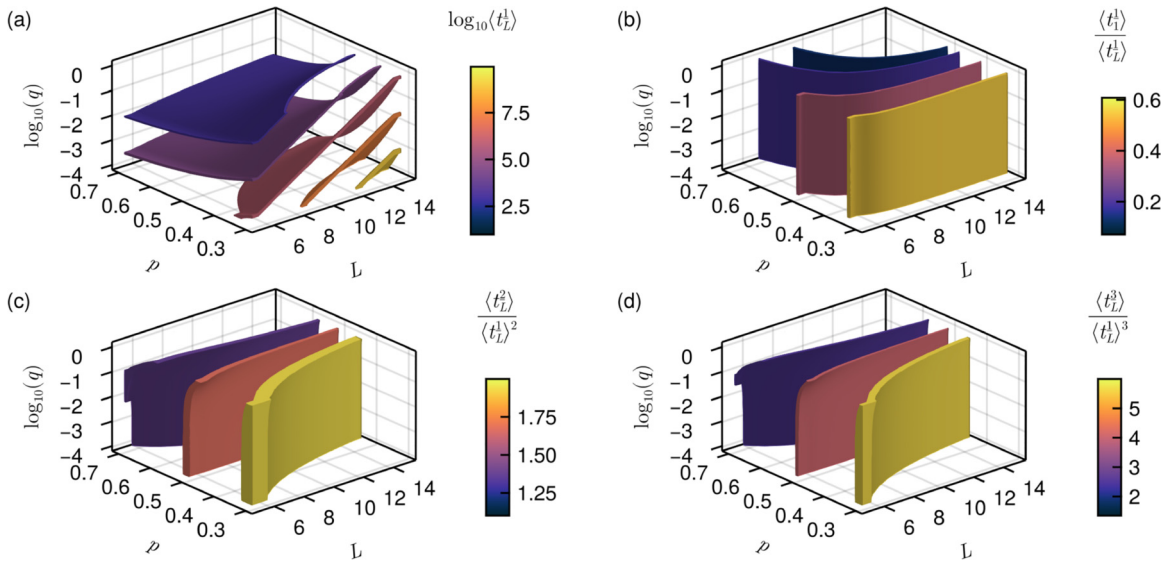

FIG. 4. Isosurfaces of constant first-passage quantities in the (L, p, q) phase space. Each surface corresponds to a fixed value of a given FPT observable, with color indicating the specific isovalue. (a) Logarithm of the first factorial moment, $\log_{10}(\langle t_L^1\rangle)$. As predicted by Eq. (7), all isosurfaces are parallel, reflecting the linear dependence on the first factorial moment of the waiting time $\langle \tau_w^1\rangle = \frac{1}{q}$. (b) Ratio $\frac{\langle t_1^1\rangle}{\langle t_L^1\rangle}$, comparing first factorial moments for walkers starting near the root versus from the leaves. (c) Normalized second factorial moment, $\frac{\langle t_L^2\rangle}{\langle t_L^1\rangle^2}$. (d) Normalized third factorial moment, $\frac{\langle t_L^3\rangle}{\langle t_L^1\rangle^3}$. Panels (c) and (d) show that the surfaces quickly lose their dependence on the waiting probability q at low values of q, making them less informative in that regime. Additionally, the similarity in behavior suggests that factorial moments beyond the second contribute little new information for structural inference.

tion. Since one can assume that the waiting-time distribution depends on at least one parameter, this implies that $k \geqslant 2$ and the inequality reduces to $n(k-\ell) \geqslant 2$. A detailed exploration of this idea lies beyond the scope of this paper.

Example: Geometric waiting—Higher moments do not reveal additional information

In this subsection, the determination of structural parameters of the tree from the factorial moments is exemplified using one of the simplest cases: a walker that moves spontaneously. That is, at each discrete-time step, the walker takes a step with probability q or remains at the current node with probability $1-q$. The resulting waiting times are geometrically distributed as defined in Eq. (11), and their factorial moments are given by $\langle \tau_w^n\rangle = n!\,\frac{(1-q)^{n-1}}{q^n} = n!\,(1-q)^{n-1}\langle \tau_w^1\rangle^n$. This system closely resembles the one studied in Refs. [14,34], where the total probability of leaving the deepest level was also treated as a tunable parameter.

Figure 4 shows isosurfaces of the factorial moments in the three-dimensional phase space spanned by the structural parameters p and L and the moving probability q. The isosurfaces of the logarithm of the first FPTFM starting from the deepest level $\langle t_L^1\rangle$, shown in Fig. 4(a), are all parallel, as predicted by Eq. (7). Furthermore, for a fixed value of $\langle t_L^1\rangle$ (e.g., obtained from a measurement), the function $\log_{10}(q(p,L))$ is proportional to the first FPTFM without waiting, $\langle \mathfrak{t}_L^1\rangle(p,L)$. This suggests that in Ref. [14], the intersection of contour lines of the MFPT measured at different laziness levels (i.e., moving probabilities) at a unique (p,L) pair is solely due to changes in the probability of leaving the deepest level. In that study, these changes were not proportional to changes in the moving probability at all other levels. It is also worth noting that $\log_{10}(q) \propto -\log_{10}\langle \tau_w^1\rangle$, so a qualitatively similar plot would be obtained for any waiting-time distribution if $\log_{10}\langle \tau_w^1\rangle$ is used as the vertical axis.

In Fig. 4(b), isosurfaces of the ratio of the first FPTFMs starting from the level below the root and from the deepest level are shown. These isosurfaces are aligned parallel to the $\log_{10}(q)$ axis, as predicted by Eq. (7). This behavior arises because, in the ratio, the contributions from the waiting-time distribution cancel out. As a result, the ratio depends solely on the structural parameters of the tree and not on the specific form of the waiting-time distribution. This cancellation property holds generally, regardless of the particular choice of $w(t)$.

From Figs. 4(c) and 4(d), which display the second and third normalized FPTFMs, it can be observed that these quantities lose their dependence on the stepping probability q as $q \to 0$, i.e., as the mean waiting time $\langle \tau_w^1\rangle \to \infty$. This behavior can be generalized using Eq. (7), which shows that it holds for all higher normalized factorial moments and that

$$\frac{\langle t^m\rangle}{\langle t^1\rangle^m} \xrightarrow{q\to 0} \sum_{\mathbf{b}\in B_m} M_{\mathbf{b}}^m \frac{\langle \mathfrak{t}^{\|\mathbf{b}\|_1}\rangle}{\langle \mathfrak{t}^1\rangle^m}, \tag{15}$$

with relative deviation from the limit bounded by $1-(1-q)^m$. As $\frac{\langle t^m\rangle}{\langle t^1\rangle^m}$ converges to a weighted sum of the FPTFMs $\langle \mathfrak{t}^k\rangle$ of the walk without waiting, any information about the

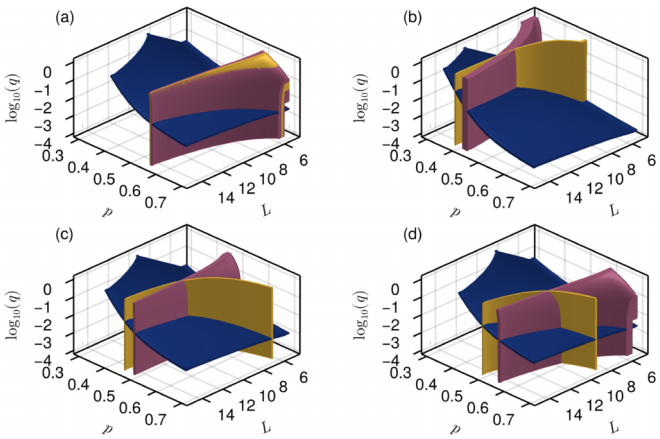

FIG. 5. Isosurfaces of constant first-passage quantities in the (L, p, q) phase space. The intersection point of the three surfaces identifies the parameters L, p, and q. This provides a 3D analog to the contour plots shown in Figs. 3(e) and 3(f). (a) Isosurfaces for the logarithm of the first factorial moment $\log_{10}(\langle t_L^1\rangle)$ (blue), the second normalized factorial moment $\frac{\langle t_L^2\rangle}{\langle t_L^1\rangle^2}$ (red), and the third normalized factorial moment $\frac{\langle t_L^3\rangle}{\langle t_L^1\rangle^3}$ (yellow). The values these quantities attain belong to a system with $p=0.6$, $L=10$, and $q=0.01$. As the second and third normalized moments produce nearly overlapping surfaces, measuring these three quantities does not allow for a unique reconstruction of the tree parameters in this regime. (b)–(d) Isosurfaces for $\log_{10}(\langle t_L^1\rangle)$ (blue), $\frac{\langle t_L^2\rangle}{\langle t_L^1\rangle^2}$ (red), and the ratio $\frac{\langle t_1^1\rangle}{\langle t_L^1\rangle}$ (yellow). The values these quantities attain belong to a system with $L=10$, $q=0.01$, and (b) $p=0.4$, (c) $p=0.5$, and (d) $p=0.6$. In panels (b)–(d), the three surfaces intersect at a single point, confirming that the combination of these observables enables unambiguous determination of L, p, and q.

waiting-time distribution is effectively lost. This renders normalized factorial moments beyond the second ineffective for inferring properties of the waiting dynamics. The details of this limiting behavior are provided in the Appendix.

This circumstance is illustrated in Fig. 5(a), where the isosurfaces of $\log_{10}\langle t^1\rangle$, $\frac{\langle t_L^2\rangle}{\langle t_L^1\rangle^2}$, and $\frac{\langle t_L^3\rangle}{\langle t_L^1\rangle^3}$ are shown for the values they attain in a system with $p=0.6$, $L=10$, and $q=0.01$. The isosurfaces of $\frac{\langle t_L^2\rangle}{\langle t_L^1\rangle^2}$ and $\frac{\langle t_L^3\rangle}{\langle t_L^1\rangle^3}$ nearly coincide; thus, if only these quantities are available, the parameters of the underlying system cannot be uniquely recovered. However, such measurements do constrain the system to a one-dimensional manifold in the (p, L, q) space given by the intersection of the $\log_{10}\langle t^1\rangle$ isosurface with the $\frac{\langle t_L^2\rangle}{\langle t_L^1\rangle^2}$ or $\frac{\langle t_L^3\rangle}{\langle t_L^1\rangle^3}$ isosurface.

Since the factorial moments beyond the second fail to provide additional information, other quantities—such as the ratio $\frac{\langle t_1^1\rangle}{\langle t_L^1\rangle}$, representing the first FPTFMs starting from the highest and deepest levels—must be used to uniquely recover the parameters p and L (and q). The same limitations discussed in Sec. III for the case without waiting also apply here. Figures 5(b) to 5(d) show the isosurfaces of $\log_{10}\langle t_L^1\rangle$, $\frac{\langle t_L^2\rangle}{\langle t_L^1\rangle^2}$, and $\frac{\langle t_1^1\rangle}{\langle t_L^1\rangle}$, each plotted for the values these quantities attain in systems with $L=10$, $q=0.01$, and $p=0.4$, $p=0.5$, and $p=0.6$, respectively. In all cases, the three isosurfaces intersect at a single point—corresponding exactly to the parameter set from which the values were derived. This demonstrates that measuring these three quantities suffices to uniquely identify the underlying tree parameters.

We emphasize that the loss of informativeness of higher moments is not limited to cases where the waiting-time distribution itself has diverging higher moments. For example, in the geometric distribution considered in this section, all factorial moments are finite, yet the higher moments of the FPT distribution become noninformative when q is small. The q-threshold at which this occurs increases for larger L or smaller p.

V. FOURIER ANALYSIS/EMPIRICAL CHARACTERISTIC FUNCTION ESTIMATION

As laid out in the previous section, in the presence of waiting, measurements of the FPTFMs for a single initial condition are not sufficient to uniquely determine all parameters of the random motion. The goal of this section is to overcome this shortcoming by employing the Fourier transform of the measured FPT distribution—also known as the empirical characteristic function [54]. This approach remains viable even in cases involving fat-tailed waiting-time distributions, where moments of sufficient order do not exist. In fact, the method of fitting the characteristic function has been known for decades and was originally introduced to estimate the parameters of stable distributions [55–58].

To assess the applicability of this approach, first-passage-time samples are generated using Monte Carlo simulations. The normalized histogram of the simulated FPTs is then Fourier transformed using the fast Fourier transform (FFT) algorithm, yielding estimates of the Fourier transform $\breve{f}(\omega_k)$ at frequencies $\omega_k=\frac{2\pi k}{t_{\max}+1}$, where $k\in\{0,1,\ldots,t_{\max}\}$, and $t_{\max}$ denotes the maximum FPT observed in the sample. An analytical expression for the Fourier transform $\tilde{f}_L(\omega)$ is available through the generating function relation $\tilde{f}_L(\omega)=\sum_{t\geqslant 0} f_L(t)e^{-i\omega t}=\hat{f}_L(e^{-i\omega})$, as provided in Eq. (9). The objective is to determine the parameters of the random motion by minimizing the mean-squared deviation

$$R^2=\frac{1}{|\Omega|}\sum_{\omega\in\Omega}|\tilde{f}(\omega)-\breve{f}(\omega)|^2, \tag{16}$$

where Ω is the set of frequency modes included in the comparison. This metric quantifies the discrepancy between the analytical and empirical Fourier transforms.

Since the histogram approximates the FPT distribution with finite accuracy—specifically, the number of observed samples at time t follows a Poisson distribution with mean $Nf(t)$, where N is the total number of samples—the estimated Fourier transform $\breve{f}$ is subject to statistical fluctuations and is not reliable for all frequency modes. A straightforward calculation shows that $\langle\breve{f}(\omega)\rangle=\tilde{f}(\omega)$, and the variance satisfies $\langle(\breve{f}(\omega)-\tilde{f}(\omega))^2\rangle\leqslant\frac{1}{N}$. This implies that indiscriminately including all Fourier modes in the error metric R^2 is not advisable, as many may be dominated by noise. To mitigate this, the frequency set Ω used in the minimization should be

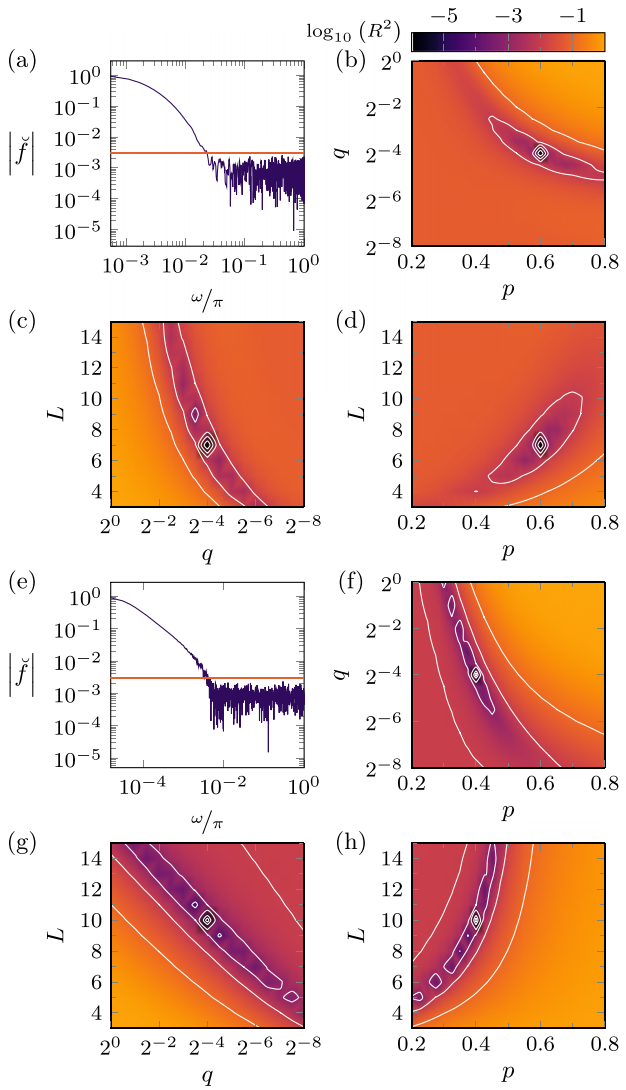

FIG. 6. Fourier mode analysis of FPT distributions obtained from Monte Carlo simulations for geometrically distributed waiting times. (a) Absolute values of the Fourier modes of the FPT distribution, computed from $N = 10^6$ trajectories. The horizontal line indicates the threshold for selecting significant modes used in the comparison with analytical predictions. (b)–(d) Phase diagrams showing the mean-squared deviation R^2 between the measured and analytical Fourier modes, as a function of model parameters. White lines represent contours of constant R^2. Default parameters are $p = 0.6$, $L = 7$, and $q = 2^{-4}$, unless otherwise varied. (e)–(h) Same analysis as in panels (a)–(d), but using simulations with $p = 0.4$, $L = 10$, and $q = 2^{-4}$. In both cases, R^2 exhibits a clear global minimum at the true parameter values used for the simulations, indicating the capacity of the method to reliably recover the underlying model. Minor local minima are also present but are comparatively shallow.

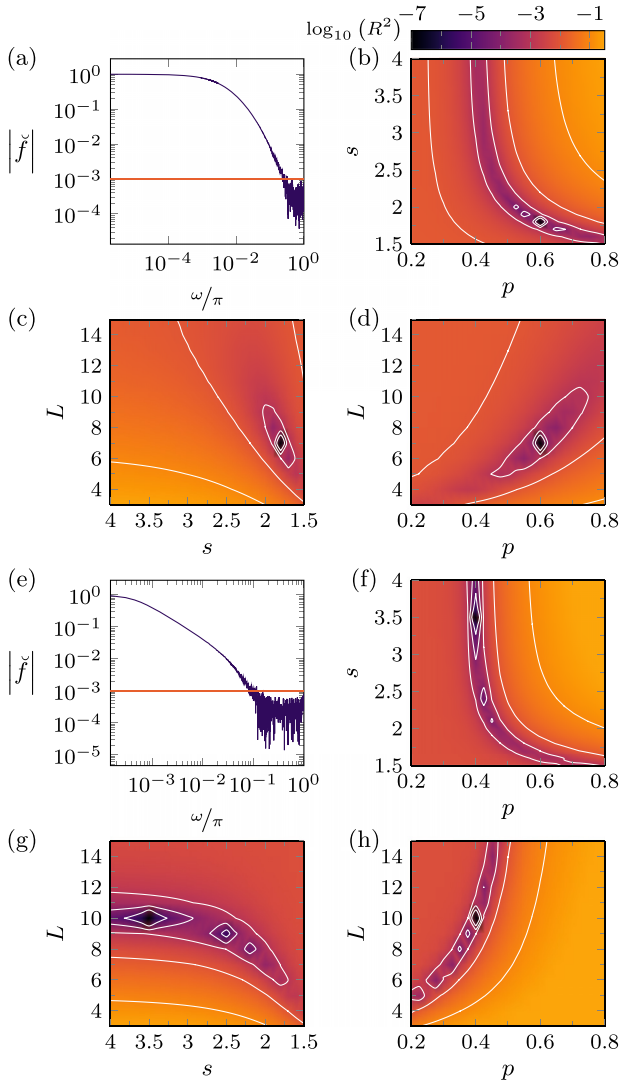

FIG. 7. Fourier mode analysis of FPT distributions obtained from Monte Carlo simulations for power-law waiting-time distributions. (a) Absolute values of the Fourier modes of the FPT distribution, computed from $N = 10^7$ trajectories. The horizontal line indicates the threshold for selecting significant modes used in the comparison with analytical predictions. (b)–(d) Phase diagrams showing the mean-squared deviation R^2 between the measured and analytical Fourier modes, as a function of model parameters. White lines represent contours of constant R^2. Default parameters are $p = 0.6$, $L = 7$, and $s = 1.8$, unless otherwise varied. (e)–(h) Same analysis as in panels (a)–(d), but using simulations with $p = 0.4$, $L = 10$, and $s = 3.5$. In both cases, R^2 exhibits a clear global minimum at the true parameter values used for the simulations, indicating the capacity of the method to reliably recover the underlying model. Minor local minima are also present but are comparatively shallow.

restricted to modes with sufficient signal strength:

$$\Omega = \{\omega_k;\ k \in \{0, 1, \ldots, t_{\max}\} \text{ and } |\check{f}(\omega_k)| > \epsilon\}, \qquad (17)$$

where $\epsilon > \frac{1}{\sqrt{N}}$ is a threshold chosen to exclude noisy modes. This approach ensures that the fit prioritizes reliable frequency components [see panels (a) and (e) of Figs. 6 and 7].

Figures 6(b)–6(d) and 6(f)–6(g) show the mean quadratic deviation R^2 computed from numerical data for two parameter sets of a walk with geometrically distributed waiting times. Orthogonal slices through the corresponding point in parameter space reveal that R^2 exhibits a sharp global minimum at the true parameter values. However, several local minima also appear, emphasizing the need for careful optimization when minimizing R^2 to estimate model parameters. This issue

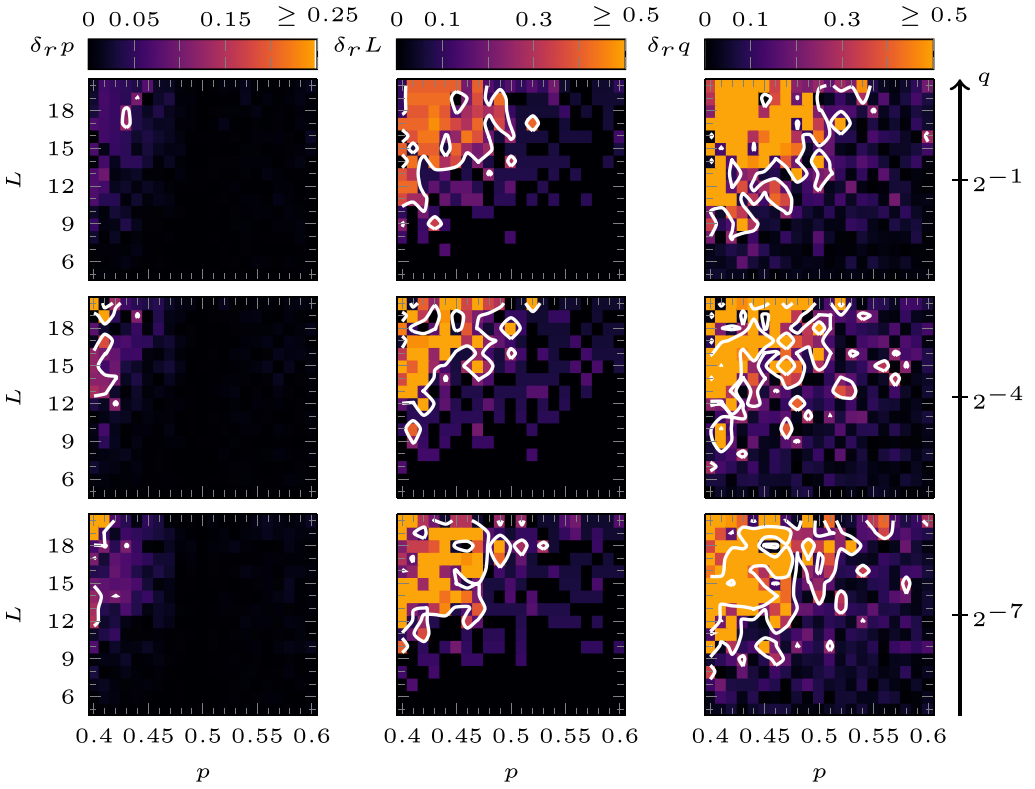

FIG. 8. Relative estimation errors for the model parameters p, L, and q as a function of true values of p and L, for different levels of moving probability q. Each row corresponds to a different value of q: $q = 2^{-1}$ (top), $q = 2^{-4}$ (middle), and $q = 2^{-7}$ (bottom). Columns show the relative deviation for: the upward bias p (first column), the tree depth L (second column), and the trap probability q (third column). Contour lines indicate levels of relative deviation: For $\delta_r p$, contours are at 0.1, for $\delta_r L$ contours are at 0.2, and for $\delta_r q$ contours are at 0.2 and 1.0. Regions with deviations exceeding 0.25 (for p) and 0.5 (for L and q) are shaded in the lightest color. Overall, p is reliably estimated across the parameter space. However, estimation accuracy for L and q decreases significantly when $p < 0.5$, particularly for larger tree depths and smaller values of q. A strong correlation is observed between the errors in L and q, suggesting interdependence in their estimation.

becomes more pronounced for bias values $p < 0.5$ and larger tree depths L. Moreover, regardless of whether $p < 0.5$ or $p > 0.5$, the minimum in the q-L section tends to be elongated along one direction, indicating that variations in q and L can lead to similar FPT distributions.

Figure 7 presents plots analogous to Fig. 6, but for a random walk with power-law distributed waiting times, $w(t) \propto \frac{1}{t^s}$. Panels (a)–(d) correspond to $s = 1.8$, where even the mean waiting time does not exist. Panels (e)–(h) show results for $s = 3.5$, where only the third and higher moments diverge. Despite the heavy tails, the mean-squared deviation R^2 still exhibits a sharp global minimum at the true parameter values, though several local minima are also present. In this case, the waiting-time exponent s and the bias parameter p can compensate for each other, leading to similar FPT distributions when varied jointly.

The behavior of the mean quadratic deviation R^2 shown in Figs. 6 and 7 is promising, suggesting that the global minimum corresponding to the true parameters of the walk can indeed be found using an optimization algorithm. As a proof of concept, R^2 was minimized for a dataset of 7056 precomputed histograms of FPTs, covering the parameter ranges $0.4 \leqslant p \leqslant 0.6$, $5 \leqslant L \leqslant 20$, and $2^{-10} \leqslant q \leqslant 1$. The estimated parameters were then compared to the true parameters used to generate each histogram. For this task, differential evolution was employed—an optimization algorithm that does not rely on gradient information and is well-suited to finding global minima in the presence of local minima [59]. This choice was arbitrary; other optimization strategies may also perform well or even better in this context.

Figure 8 shows the relative deviations of the estimated parameters from their true values on p-L sections of the phase space for different values of the moving probability q. The results indicate that the bias probability p can be estimated with high accuracy, with relative deviations typically below 5%. In contrast, accurate estimation of q and L is more sensitive. Low deviations in these parameters are generally achieved only when $p > 0.5$ or when the depth L is small. For $p < 0.5$ and sufficiently large L, the relative deviations in both L and q become significant and tend to increase further as q decreases.

We note that the empirical characteristic function approach is indeed a reliable tool for parameter estimation in cases where the distribution is only described through its characteristic function [58]. Since, for any waiting-time distribution with a known characteristic function, the characteristic function of the corresponding FPT distribution can be derived analytically, we expect the empirical characteristic function approach to be in principle generalizable beyond the geometric and power-law cases considered here.

VI. CONCLUSION AND OUTLOOK

We developed a framework for inferring the structure of nonuniform finite Cayley trees from first-passage-time statistics. We showed that the first two factorial moments of FPTs are sufficient to uniquely determine the depth and geometric bias of the tree in the absence of trapping effects. When traps or sticky regions are present, we demonstrated that the generating function of the FPT distribution is the composition of the generating functions of the FPT distribution without waiting and the waiting-time distribution. This decomposition leads to a nonlinear system of equations connecting factorial moments across different scenarios. We further explored strategies to resolve this inverse problem under trapping conditions. In particular, we found that varying the initial position of the random walker or analyzing the Fourier transform of the FPT distribution allows successful inference even for power-law waiting-time distributions, where traditional moment-based approaches fail due to divergence of higher-order moments.

In the present work, we considered the case of absorbing site being located at the root. However, more generally, the target can be placed at an arbitrary node. To discuss the possibility of handling such scenarios, we note that previous numerical studies in the context of neuronal dendrites [14,34] have shown that for moderate deviations from a perfectly regular Cayley tree, the MFPT deviates only mildly from the effective value obtained for the regular case. This suggests that the inference framework should remain reasonably robust even when the absorbing site is not located at the root. When the target is placed at another node, two cases for the bias of the motion can be distinguished: (i) Bias directed toward the target site: In this case, the tree can be reordered so that the target becomes the new root. This results in an irregular structure, to which the considerations above apply. (ii) Bias directed toward the root: Here the situation is more involved. Since the level of the particle alone is insufficient to determine arrival at the target, the process can no longer be mapped onto a simple 1D walk. However, the structure can still be decomposed into a full $(\mathfrak{z}-1)$-ary child tree below the target ($\mathfrak{z}$ being the coordination number) and segments between the target and the root, connected to $(\mathfrak{z}-1)$-ary subtrees of varying depths. These subtrees can be considered as traps, allowing to map the structure between target and the root onto a 1D random walk with site-dependent waiting probabilities. Such a decomposition might allow for the formulation of renewal-type equations for the FPT distribution to an arbitrary target site.

Our analysis revealed that the empirical characteristic function estimation does not always provide accurate estimates for the parameters L and q across the full parameter space. To mitigate this, we selected a very low threshold value for significant modes, thereby retaining more information and reducing the regions where estimation fails. Nevertheless, as an interesting avenue for future research, further work is needed to better understand which modes are essential for obtaining robust estimates of p, L, and q.

Our results offer new tools for structural inference across a broad class of branched systems—from biological networks such as bronchial, vascular, and neuronal dendritic trees to synthetic and engineered systems like communication, utility, and transportation networks. The proposed method enables noninvasive characterization of network structures in scenarios where direct imaging or tracer tracking is challenging or infeasible. While our study focused on treelike networks, the underlying ideas are extendable to more complex architectures, including graphs with loops or hybrid tree-graph topologies. Future extensions may incorporate irregular or weighted networks, as well as scenarios involving noisy or incomplete first-passage time data. These directions naturally lend themselves to integration with statistical inference techniques or machine learning methods, broadening the applicability of our framework. By linking random walk dynamics with inverse structural inference, our approach adds to the growing repertoire of tools for uncovering hidden features of complex systems through stochastic observations.

ACKNOWLEDGMENTS

We thank Matthias K. Hoffmann for fruitful discussions. This work was supported by the Deutsche Forschungsgemeinschaft (DFG) within the collaborative research center SFB 1027 and also via Grant No. INST 256/539-1, which funded the computing resources at Saarland Uniono. R.S. acknowledges support by the Young Investigator Grant of Saarland University, Grant No. 7410110401.

DATA AVAILABILITY

The data that support the findings of this article are openly available [60].

APPENDIX: DERIVATION OF EQ. (15) AND THE ERROR BOUND

In this Appendix, we derive Eqs. (7) and (15), as well as the estimate for the relative deviation.

Equation (7) expresses the FPTFMs of a random walk with waiting in terms of the FPTFMs of the walk without waiting $\langle \mathfrak{t}^{\underline{k}} \rangle$ and the factorial moments of the waiting-time distribution $\langle \tau_w^{\underline{k}} \rangle$. It follows from applying Eq. (3) to Eq. (6). For the nth FPTFM $\langle t^{\underline{n}} \rangle$, one requires the nth derivative of a composite function. Using the notation of Eq. (7), this derivative can be written as

$$\frac{\mathrm{d}^n}{\mathrm{d}z^n}\hat{\mathfrak{f}}(\hat{w}(z)) = \sum_{\mathbf{b}\in B_n} M_{\mathbf{b}}^n \hat{\mathfrak{f}}^{(\|\mathbf{b}\|_1)}(\hat{w}(z)) \prod_{j=1}^{n} \left(\frac{\hat{w}^{(j)}(z)}{j!} \right)^{b_j},$$

where the superscript in parenthesis denotes higher derivatives, which is a standard form of Faà di Bruno's formula; see, e.g., Ref. [41]. Evaluating this expression at $z=1$ gives $\langle t^{\underline{n}} \rangle$. Since $\hat{w}(1)=1$ by normalization, we have $\hat{\mathfrak{f}}^{(k)}(1) = \langle \mathfrak{t}^{\underline{k}} \rangle$ and $\hat{w}^{(k)} = \langle \tau_w^{\underline{k}} \rangle$, which directly yields Eq. (7).

Next, we derive Eq. (15). By applying Eq. (7) to both the numerator and denominator, and using $\langle \tau_w^{\underline{1}} \rangle^m = \prod_{k=1}^m \langle \tau_w^{\underline{1}} \rangle^{k b_k}$ in the sum, the normalized FPTFM with waiting can be written, using the notation introduced in Eq. (7), as

$$\begin{aligned} \frac{\langle t^{\underline{m}} \rangle}{\langle t^{\underline{1}} \rangle^m} &= \sum_{\mathbf{b}\in B_m} M_{\mathbf{b}}^m \frac{\langle \mathfrak{t}^{\underline{\|\mathbf{b}\|_1}} \rangle}{\langle \mathfrak{t}^{\underline{1}} \rangle^m} \frac{\prod_{k=1}^m \left(\frac{\langle \tau_w^{\underline{k}} \rangle}{k!} \right)^{b_k}}{\langle \tau_w^{\underline{1}} \rangle^m} \\ &= \sum_{\mathbf{b}\in B_m} M_{\mathbf{b}}^m \frac{\langle \mathfrak{t}^{\underline{\|\mathbf{b}\|_1}} \rangle}{\langle \mathfrak{t}^{\underline{1}} \rangle^m} \prod_{k=1}^{m} \left(\frac{\langle \tau_w^{\underline{k}} \rangle}{k! \langle \tau_w^{\underline{1}} \rangle^k} \right)^{b_k}, \end{aligned} \tag{A1}$$

independent of the chosen waiting-time distribution.

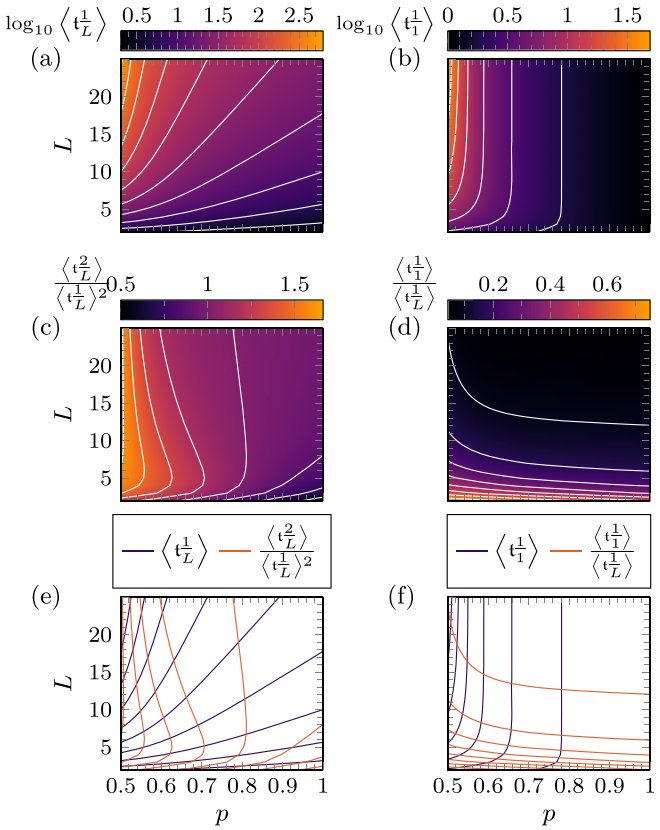

FIG. 9. Same analysis as in Fig. 3, but restricted to the regime $p \geqslant 0.5$, with contour levels adjusted to match the narrower range of deviations.

Recalling that for spontaneous stepping the normalized factorial moments of the waiting-time distribution are given by $\frac{\langle \tau_w^k \rangle}{\langle \tau_w^1 \rangle^k} = k!(1-q)^{k-1}$, the expression simplifies further to

$$\frac{\langle t^{\underline{m}} \rangle}{\langle t^1 \rangle^m} = \sum_{\mathbf{b} \in B_m} M_{\mathbf{b}}^m \frac{\langle \mathrm{t}^{\underline{\|\mathbf{b}\|_1}} \rangle}{\langle \mathrm{t}^1 \rangle^m} \frac{(1-q)^m}{(1-q)^{\|\mathbf{b}\|_1}}$$

$$\begin{cases} \leqslant \sum_{\mathbf{b} \in B_m} M_{\mathbf{b}}^m \frac{\langle \mathrm{t}^{\underline{\|\mathbf{b}\|_1}} \rangle}{\langle \mathrm{t}^1 \rangle^m}, \\ \geqslant (1-q)^m \sum_{\mathbf{b} \in B_m} M_{\mathbf{b}}^m \frac{\langle \mathrm{t}^{\underline{\|\mathbf{b}\|_1}} \rangle}{\langle \mathrm{t}^1 \rangle^m}. \end{cases} \tag{A2}$$

For the "$\leqslant$" part of Eq. (A2), we use that $\|\mathbf{b}\|_1 \leqslant m$, which implies that every summand is positive and bounded above by $M_{\mathbf{b}}^m \frac{\langle \mathrm{t}^{\underline{\|\mathbf{b}\|_1}} \rangle}{\langle \mathrm{t}^1 \rangle^m}$. For the "$\geqslant$" part, observe that $0 < 1-q \leqslant 1$, so for any exponent $\nu \in \mathbf{N}$, we have $1 \leqslant \frac{1}{(1-q)^\nu} < \infty$. Therefore, omitting the factor $\frac{1}{(1-q)^{\|\mathbf{b}\|_1}}$ from each summand decreases its value or leaves it unchanged, which justifies the lower bound. From Eq. (A2) it follows that

$$\frac{\langle t^{\underline{m}} \rangle}{\langle t^1 \rangle^m} \xrightarrow{q \to 0} \sum_{\mathbf{b} \in B_m} M_{\mathbf{b}}^m \frac{\langle \mathrm{t}^{\underline{\|\mathbf{b}\|_1}} \rangle}{\langle \mathrm{t}^1 \rangle^m},$$

and the relative deviation from the limit is given by $1 - (1-q)^m \overset{q \ll 1}{\sim} mq$.

As $\langle \mathrm{t}^1 \rangle \to \infty$, the normalized factorial moments $\frac{\langle t^{\underline{m}} \rangle}{\langle t^1 \rangle^m}$ remain bounded [cf. Fig. 3 and Figs. 4(c) and 4(d)], implying that $\langle \mathrm{t}^{\underline{m}} \rangle \sim \langle \mathrm{t}^1 \rangle^m$ in this limit. Since $\|\mathbf{b}\|_1 \leqslant m$ for all $\mathbf{b} \in B_m$, it follows that

$$\lim_{q \to 0} \frac{\langle t^{\underline{m}} \rangle}{\langle t^1 \rangle^m} \overset{\langle \mathrm{t}^1 \rangle \gg 1}{\sim} \frac{\langle \mathrm{t}^{\underline{m}} \rangle}{\langle \mathrm{t}^1 \rangle^m}$$

in the small q limit. This explains why in Figs. 4(b) and 4(d) the isosurfaces appear nearly invariant with respect to q when $p < 0.5$.

[1] D. ben Avraham and S. Havlin, *Diffusion and Reactions in Fractals and Disordered Systems* (Cambridge University Press, Cambridge, UK, 2000).

[2] R. Krishna, Describing the diffusion of guest molecules inside porous structures, J. Phys. Chem. C **113**, 19756 (2009).

[3] R. W. Mair, G. P. Wong, D. Hoffmann, M. D. Hürlimann, S. Patz, L. M. Schwartz, and R. L. Walsworth, Probing porous media with gas diffusion NMR, Phys. Rev. Lett. **83**, 3324 (1999).

[4] P. P. Mitra, P. N. Sen, L. M. Schwartz, and P. Le Doussal, Diffusion propagator as a probe of the structure of porous media, Phys. Rev. Lett. **68**, 3555 (1992).

[5] F. F. Chen and Y. S. Yang, Microstructure-based characterization of permeability using a random walk model, Model. Simul. Mater. Sci. Eng **20**, 045005 (2012).

[6] P. Tierno and M. R. Shaebani, Enhanced diffusion and anomalous transport of magnetic colloids driven above a two-state flashing potential, Soft Matter **12**, 3398 (2016).

[7] M. Kac, Can one hear the shape of a drum? Am. Math. Month. **73**, 1 (1966).

[8] M. Felici, M. Filoche, and B. Sapoval, Renormalized random walk study of oxygen absorption in the human lung, Phys. Rev. Lett. **92**, 068101 (2004).

[9] Z. Sadjadi, M. F. Miri, M. R. Shaebani, and S. Nakhaee, Diffusive transport of light in a two-dimensional disordered packing of disks: Analytical approach to transport mean free path, Phys. Rev. E **78**, 031121 (2008).

[10] D. J. Durian, D. A. Weitz, and D. J. Pine, Multiple light-scattering probes of foam structure and dynamics, Science **252**, 686 (1991).

[11] G. Maret, Diffusing-wave spectroscopy, Curr. Opin. Colloid Interface Sci. **2**, 251 (1997).

[12] C. Cooper, T. Radzik, and S. Y., Fast low-cost estimation of network properties using random walks, Internet Math. **12**, 221 (2016).

[13] E. Agliari, R. Burioni, D. Cassi, and F. M. Neri, Autocatalytic reaction on low-dimensional substrates, Theor. Chem. Acc. **118**, 855 (2007).

[14] R. Jose, L. Santen, and M. R. Shaebani, Trapping in and escape from branched structures of neuronal dendrites, Biophys. J. **115**, 2014 (2018).

[15] N. Spruston, Pyramidal neurons: Dendritic structure and synaptic integration, Nat. Rev. Neurosci. **9**, 206 (2008).

[16] H. Hering and M. Sheng, Dendritic spines: Structure, dynamics and regulation, Nat. Rev. Neurosci. **2**, 880 (2001).

[17] P. Vetter, A. Roth, and M. Häusser, Propagation of action potentials in dendrites depends on dendritic morphology, J. Neurophysiol. **85**, 926 (2001).

[18] F. Kreten, B. Niemeyer, L. Santen, and R. Shaebani, Tracking the morphological evolution of neuronal dendrites by first-passage analysis, https://www.biorxiv.org/content/10.1101/2024.10.13.618072v2.full.

[19] I. Rodríguez-Iturbe and A. Rinaldo, *Fractal River Basins: Chance and Self-Organization* (Cambridge University Press, Cambridge, UK, 2001).

[20] J. R. Banavar, A. Maritan, and A. Rinaldo, Size and form in efficient transportation networks, Nature (London) **399**, 130 (1999).

[21] E. Helfand and D. S. Pearson, Statistics of the entanglement of polymers: Unentangled loops and primitive paths, J. Chem. Phys. **79**, 2054 (1983).

[22] B. Wu, Y. Lin, Z. Zhang, and G. Chen, Trapping in dendrimers and regular hyperbranched polymers, J. Chem. Phys. **137**, 044903 (2012).

[23] D.-J. Heijs, V. A. Malyshev, and J. Knoester, Trapping time statistics and efficiency of transport of optical excitations in dendrimers, J. Chem. Phys. **121**, 4884 (2004).

[24] D. Katsoulis, P. Argyrakis, A. Pimenov, and A. Vitukhnovsky, Diffusion and trapping in dendrimer structures, Chem. Phys. **275**, 261 (2002).

[25] P. Argyrakis and R. Kopelman, Random walks and reactions on dendrimer structures, Chem. Phys. **261**, 391 (2000).

[26] J. F. Gouyet, V. Fleury, J.-F. Gouyet, and M. Leonetti, *Branching in Nature: Dynamics and Morphogenesis of Branching Structures, From Cell to River Networks* (Springer-Verlag, Berlin, 2001).

[27] M. E. J. Newman, *Networks: An Introduction* (Oxford University Press, New York, NY, 2010).

[28] R. Pastor-Satorras, C. Castellano, P. Van Mieghem, and A. Vespignani, Epidemic processes in complex networks, Rev. Mod. Phys. **87**, 925 (2015).

[29] J. M. Kleinberg, Navigation in a small world, Nature (London) **406**, 845 (2000).

[30] G. Szabó, M. Alava, and J. Kertész, Shortest paths and load scaling in scale-free trees, Phys. Rev. E **66**, 026101 (2002).

[31] B. Bollobás and O. Riordan, Shortest paths and load scaling in scale-free trees, Phys. Rev. E **69**, 036114 (2004).

[32] E. Agliari, A. Blumen, and O. Mülken, Dynamics of continuous-time quantum walks in restricted geometries, J. Phys. A **41**, 445301 (2008).

[33] R. Metzler, S. Redner, and G. Oshanin, *First-Passage Phenomena and Their Applications* (World Scientific, Singapore, 2014), pp. 96–121.

[34] M. R. Shaebani, R. Jose, C. Sand, and L. Santen, Unraveling the structure of treelike networks from first-passage times of lazy random walkers, Phys. Rev. E **98**, 042315 (2018).

[35] S. Redner, *A Guide to First-Passage Processes* (Cambridge University Press, Cambridge, UK, 2001).

[36] B. D. Hughes and M. Sahimi, Random walks on the Bethe lattice, J. Stat. Phys. **29**, 781 (1982).

[37] C. Monthus and C. Texier, Random walk on the Bethe lattice and hyperbolic Brownian motion, J. Phys. A **29**, 2399 (1996).

[38] D. Cassi, Random walks on Bethe lattices, Europhys. Lett. **9**, 627 (1989).

[39] M. Khantha and V. Balakrishnan, First passage time distributions for finite one-dimensional random walks, Pramana **21**, 111 (1983).

[40] L. Skarpalezos, A. Kittas, P. Argyrakis, R. Cohen, and S. Havlin, Anomalous biased diffusion in networks, Phys. Rev. E **88**, 012817 (2013).

[41] J. Riordan, *An Introduction to Combinatorial Analysis* (Princeton University Press, Princeton, NJ, 1980).

[42] H. S. Wilf, *Generatingfunctionology* (Academic Press, Boston, MA, 1994).

[43] P. Flajolet and R. Sedgewick, *Analytic Combinatorics* (Cambridge University Press, Cambridge, UK, 2009).

[44] N. Van Kampen, *Stochastic Processes in Physics and Chemistry* (Elsevier Science, Amsterdam, The Netherlands, 2011).

[45] A. Bialas and R. Peschanski, Moments of rapidity distributions as a measure of short-range fluctuations in high-energy collisions, Nucl. Phys. B **273**, 703 (1986).

[46] H. Risken, Reduction of the number of variables, in *The Fokker-Planck Equation: Methods of Solution and Applications* (Springer, Berlin, Heidelberg, 1996), pp. 179–195.

[47] A. Dienst and R. Friedrich, Mean first passage time for a class of non-Markovian processes, Chaos **17**, 033104 (2007).

[48] M. Manhart, W. Kion-Crosby, and A. V. Morozov, Path statistics, memory, and coarse-graining of continuous-time random walks on networks, J. Chem. Phys. **143**, 214106 (2015).

[49] The multinomial coefficient $\binom{m}{\mathbf{b}}$ has the same formula as $M^m_{\mathbf{b}}$, but also requires $m = \|\mathbf{b}\|_1$.

[50] M. Ostilli, Cayley trees and bethe lattices: A concise analysis for mathematicians and physicists, Physica A **391**, 3417 (2012).

[51] M. Roughan, The polylogarithm function in julia, arXiv:2010.09860.

[52] P. L. Mills, Numerical inversion of z-transforms with application to polymerization kinetics, Comput. Chem. **11**, 137 (1987).

[53] I. Horváth, A. Mészáros, and M. Telek, Numerical inverse transformation methods for z-transform, Mathematics **8**, 556 (2020).

[54] H. Cramer, *Mathematical Methods of Statistics* (Princeton University Press, Princeton, NJ, 1946).

[55] S. J. Press, Estimation in univariate and multivariate stable distributions, J. Am. Stat. Assoc. **67**, 842 (1972).

[56] C. R. Heathcote, The integrated squared error estimation of parameters, Biometrika **64**, 255 (1977).

[57] A. S. Paulson, E. W. Holcomb, and R. A. Leitch, The estimation of the parameters of the stable laws, Biometrika **62**, 163 (1975).

[58] J. Yu, Empirical characteristic function estimation and its applications, Econom. Rev. **23**, 93 (2004).

[59] R. Storn and K. Price, Differential evolution—A simple and efficient heuristic for global optimization over continuous spaces, J. Global Optim. **11**, 341 (1997).

[60] M. R. Shaebani, Inferring tree structure with hidden traps from first passage times [Data set], Zenodo (2025), doi:10.5281/zenodo.17370310.